Hindawi
Shock and Vibration
Volume 2017, Article ID 2365812, 12 pages
https://doi.org/10.1155/2017/2365812

Research Article

Dynamic Reliability Evaluation of Road Vehicle Subjected to Turbulent Crosswinds Based on Monte Carlo Simulation

Bin Wang,[1,2] Yongle Li,[1] Helu Yu,[1] and Haili Liao[1]

[1]*Department of Bridge Engineering, Southwest Jiaotong University, Chengdu 610031, China*
[2]*Key Laboratory of Transportation Tunnel Engineering, Ministry of Education, Chengdu 610031, China*

Correspondence should be addressed to Bin Wang; wangbinwvb@home.swjtu.edu.cn

Received 17 September 2016; Revised 13 December 2016; Accepted 28 December 2016; Published 29 January 2017

Academic Editor: Sakdirat Kaewunruen

As a vehicle moves on roads, a complex vibration system of the running vehicle is formed under the collective excitations of random crosswinds and road surface roughness, together with the artificial handing by the drivers. Several numerical models in deterministic way to assess the safety of running road vehicles under crosswinds were proposed. Actually, the natural wind is a random process in time domain due to turbulence, and the surface roughness of a road is also a random process but in spatial domain. The nature of a running vehicle therefore is an extension of dynamic reliability excited by random processes. This study tries to explore the dynamic reliability of a road vehicle subjected to turbulent crosswinds. Based on a nonlinear vibration system, the dynamic responses of a road vehicle are simulated to obtain the dynamic reliability. Monte Carlo Simulation with Latin Hypercube Sampling is then applied on the possible random variables including the vehicle weight, road friction coefficient, and driver parameter to look at their effects. Finally, a distribution model of the dynamic reliability and a corresponding index for the wind-induced vehicle accident considering these random processes and variables is proposed and employed to evaluate the safety of the running vehicle.

1. Introduction

In crosswinds, road vehicles can be turned over or blown off from their original lanes [1, 2], which may lead to a huge loss of property or even bring away many lives. Therefore, the evaluation of the wind-induced performance of vehicles has been focused on continually in the last decades [3–7]. In these studies, the wind-vehicle systems are treated in deterministic ways and pairs of fixed critical wind velocity and vehicle speed are conducted. Actually, several factors such as the vehicles' parameters, the wind velocity, and the road surface roughness are random variables or processes. The critical wind velocity and vehicle speed therefore become indefinite.

A general probabilistic model for the safety of road vehicle in windy condition was presented firstly by Sigbjörnsson and Snæbjörnsson [8] to explore the indefinite in the wind-vehicle system. Like other system variables, the wind velocity was also taken as a random variable in this model. And the accident index based on the safety limit states was calculated. The system employed in this model is simplified too much, and the adoption of a more realistic dynamic vehicle model is deemed necessary particularly when complicated driving conditions are considered. Thus, F. Chen and S. Chen [9] proposed a framework of a reliability-based assessment model of the vehicle safety under complex driving environments. In this framework, response surface method was applied to approximate the reliability index as the functions of the system variables, and the wind velocity was also accepted as a random variable. In the wind-induced performance analysis on road vehicles, wind velocity is a random process rather than a random variable. Considering the wind velocity only as a random variable excludes the wind-induced dynamic effects on the vehicles in nature. Another risk assessment procedure for wind-vehicle system was reported by Proppe and Wetzel [10]. The turbulent crosswind was replaced with a gust wind model, of which the peak and duration are random variables. More complex situation like the random road roughness and driver behaviors was not explored in [8–10].

Actually, the natural wind is a random process in time domain due to the turbulence, and the surface roughness of a road is also a random process but in spatial domain. The nature of the running vehicles therefore is an extension of dynamic reliability. In this study, a nonlinear vibration control system including the random crosswind, the plane surface roughness, and the driver behavior is applied. In this system, the common linear assumption with small angular displacement is revised to consider the possible large dynamic performance. With this system, the dynamic responses of a road vehicle under the random turbulent winds are simulated. Three typical dynamic reliability evaluation methods including the first-passage, Poisson assumption, and Markov assumption are selected and compared for the wind-vehicle system. The effects of the mean wind velocity, vehicle speed, and the roughness level on the dynamic reliability are also studied. The system random variables are sampled using Latin Hypercube Sampling method. With Monte Carlo Simulation, the reliability distributions corresponding to these random variables are gotten. A distribution model with a single parameter modified on Lorentz profile is then presented. Taking this parameter as an index, the dynamic reliability of the complex wind-induced vehicle system can be evaluated. The highlights of this study are composed of three parts in brief. Firstly, the wind-vehicle accident is evaluated in the concept of dynamic reliability with a selection of reliability evaluation method. Secondly, the distributions of the dynamic reliability on several random variables of the wind-vehicle system are computed and analyzed. Finally, a distribution model with a single parameter is presented.

2. Vibration System of Road Vehicle

A nonlinear vibration system of road vehicle was established in [7]. The road vehicle is simplified as a combination of several rigid bodies, including the main vehicle body and wheels (see Figure 1). Through a few elastic connections, these rigid bodies functioned as an entire vehicle. This system can well predict the dynamic behaviors of the vehicle moving on the ground in crosswinds.

The vehicle body bears the gravity and the wind loads and receives the elastic forces from the suspension between it and the wheels (see Figure 2). Its dynamic equations of equilibrium can be expressed as

$$m_{vb}\dot{v}_{vby} + m_{vb}\omega_{vbz}v_{vbx} - m_{vb}\omega_{vbx}v_{vbz} = -\sum_{i=1}^{4} f_{wiy}^{S} - f_{vby}^{G} + f_{vy}^{W} \tag{1a}$$

$$m_{vb}\dot{v}_{vbz} - m_{vb}\omega_{vby}v_{vbx} + m_{vb}\omega_{vbx}v_{vby} = -\sum_{i=1}^{4} f_{wiz}^{S} - f_{vbz}^{G} + f_{vz}^{W} \tag{1b}$$

$$I_{xx}\dot{\omega}_{vbx} - I_{xz}\dot{\omega}_{vbz} + \left(I_{zz} - I_{yy}\right)\omega_{vby}\omega_{vbz} - I_{xz}\omega_{vbx}\omega_{vby} = m_{vx}^{W} + \sum_{i=1,2} f_{wiz}^{S} b_1 - \sum_{i=3,4} f_{wiz}^{S} b_1 - \sum_{i=1}^{4} f_{wiy}^{S} h_1 \tag{1c}$$

$$I_{yy}\dot{\omega}_{vby} + \left(I_{xx} - I_{zz}\right)\omega_{vbx}\omega_{vbz} - I_{xz}\left(\omega_{vbz}^{2} - \omega_{vbx}^{2}\right) = m_{vy}^{W} - \sum_{i=2,4} f_{wiz}^{S} L_2 + \sum_{i=1,3} f_{wiz}^{S} L_1 \tag{1d}$$

$$I_{zz}\dot{\omega}_{vbz} - I_{zx}\dot{\omega}_{vbx} + \left(I_{yy} - I_{xx}\right)\omega_{vbx}\omega_{vby} + I_{xz}\omega_{vby}\omega_{vbz} = m_{vz}^{W} - \sum_{i=1,3} f_{wiy}^{S} L_1 + \sum_{i=2,4} f_{wiy}^{S} L_2, \tag{1e}$$

where x, y, and z are the three directions in the Cartesian coordinate system founded on the gravity center of the vehicle; f_{vbj}^{G}, f_{vj}^{W}, and m_{vj}^{W} (with $j = x, y, z$) are the gravity, the wind-induced forces, and moments, representing the external loads on the vehicle; f_{wij}^{S} (with $j = y, z$) are the forces passed between the vehicle body and the ith wheel, representing the elastic and damping forces of the suspension; b_1, h_1, l_1, and l_2 are the distance components from the gravity center to the wheel centers, causing the eccentric moments of the suspension on the vehicle gravity center; m_{vb} and I_{jk} (with $j = x, y, z$ and $k = x, y, z$) are the mass and the mass moment of inertia, representing the inertia properties of the vehicle; v_{vbj}, $\dot{v}_{vbj}$, ω_{vbj}, and $\dot{\omega}_{vbj}$ (with $j = x, y, z$) are the translational and angular velocity or acceleration components, representing the motion state of the vehicle body under the crosswinds. Through the Euler angles and transformation matrix, the motion of the vehicle body can be transformed into the global coordinate system founded on the ground [7].

3. Random Process and Uncertain Variables

3.1. Random Turbulent Winds and Resultant Loads

3.1.1. Random Turbulent Winds. Turbulent winds, isolated from the mean wind, are random processes with random characteristics in both space and time domain. Generally, the auto- and cross-correlations are calculated from the observation values of the wind velocities. And the corresponding wind velocity spectrums and correlation coefficient are utilized to describe the statistic characteristics of the turbulent winds [11]. At fixed locations, the power spectrums of the turbulent winds can be described in Kaimal spectrum [12]. In Kaimal spectrum, the power spectrums of the wind

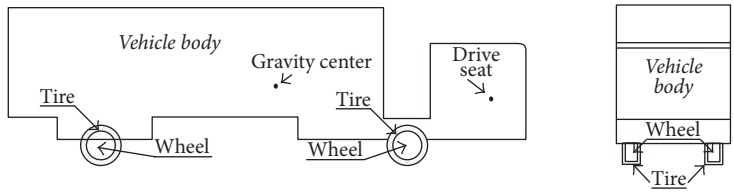

Figure 1: Simplified vehicle model.

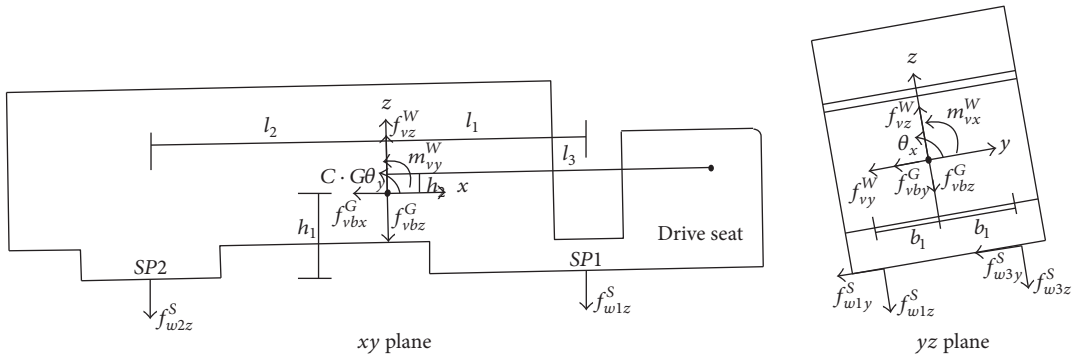

Figure 2: Force diagrams of vehicle body.

velocity component u in the direction of the mean wind and the component v in the vertical direction are

$$\frac{nS_u(f)}{u_*^2} = \frac{200f}{(1+50f)^{5/3}} \tag{2a}$$

$$\frac{nS_v(f)}{u_*^2} = \frac{15f}{(1+9.5f)^{5/3}} \tag{2b}$$

$$f = \frac{n_f z_h}{U(z_h)} \tag{2c}$$

$$u_* = \frac{KU(z_h)}{\ln(z_h/z_0)}, \tag{2d}$$

where S_u and S_v are the power spectrums of u and v, respectively, and they are the functions of a nondimensional normalized frequency f; n_f is the frequency in Hz; u_* is the shear velocity of the flow; $U(z_h)$ is the mean velocity at the height z_h; z_0 is the roughness height of the ground; and K is Von Kármán number.

For a moving body like a vehicle, the turbulent wind spectrums can be derived based on Taylor's frozen turbulence hypothesis by Taylor [13]. In this way, the power spectrums of the fluctuating winds attached on the moving vehicle based on Kaimal spectrum can be derived [14] as

$$S_i(n_f) = 4\sqrt{\frac{\pi}{2}}u_*^2\frac{z}{V_r}\left[d_i A + (1-d_i)(A-B-C-D)\right] \tag{3}$$

with

$$A = \frac{0.52017}{0.05419 + (2\pi n_f)^2} + \frac{1.20867}{1.57290 + (2\pi n_f)^2} + \frac{0.08540}{0.00404 + (2\pi n_f)^2} \tag{4a}$$

$$B = \frac{0.01409\left(1 - 18.45244(2\pi n_f)^2\right)}{\left[0.05419 + (2\pi n_f)^2\right]^2} \tag{4b}$$

$$C = \frac{0.95056\left(1 - 0.63577(2\pi n_f)^2\right)}{\left[1.57290 + (2\pi n_f)^2\right]^2} \tag{4c}$$

$$D = \frac{0.00017\left(1 - 247.81938(2\pi n_f)^2\right)}{\left[0.00404 + (2\pi n_f)^2\right]^2}, \tag{4d}$$

where $i = u$ and v, and

$$d_u = \left[\frac{(U + V\cos\varphi)}{V_r}\right]^2 \tag{5a}$$

$$d_v = \left[\frac{(V\sin\varphi)}{V_r}\right]^2 \tag{5b}$$

$$V_r = \sqrt{U^2 + V^2 + 2UV\cos\varphi}, \tag{5c}$$

where U, V, and φ are the mean wind velocity, the vehicle speed, and the angle between them.

The turbulent winds are assumed to be zero-mean stationary Gaussian random process. Given the power spectrums, the instant wind velocities at time t can be simulated through an inverse Fourier Transform as

$$u(t) = \sum_{i=1}^{i=N} \sqrt{2\Delta n_f S_u(n_i)} \cos\left[2\pi n_{fi} t + \phi_u\right] \tag{6a}$$

$$v(t) = \sum_{i=1}^{i=N} \sqrt{2\Delta n_f S_v(n_i)} \cos\left[2\pi n_{fi} t + \phi_v\right], \tag{6b}$$

where Δn is the frequency interval; N is the total number of frequency intervals to be simulated; and ϕ_u and ϕ_v are random phase angles uniformly distributed between 0 and 2π.

3.1.2. Resultant Wind Loads. Actually, the turbulent winds $u(t)$ and $v(t)$ in (6a) and (6b) are generated in a global coordinate system attached on Earth. To consider the possible relative wind angles between the vehicle body and the wind, the natural wind velocities containing the turbulent winds in the global system are transformed into the wind velocities in the local coordinate system of the vehicle body $[U_{xe}, U_{ye}, U_{ze}]$ through a transformation matrix [7]. The resultant wind loads in the dynamic equations of equilibrium (see (1a), (1b), (1c), (1d), and (1e)) can be then expressed on the quasi-steady assumption as

$$f_{vy}^W = \frac{1}{2}\rho U_{re}^2 A_f C_S(\alpha_w, \beta_w) \tag{7a}$$

$$f_{vz}^W = \frac{1}{2}\rho U_{re}^2 A_f C_L(\alpha_w, \beta_w) \tag{7b}$$

$$m_{vx}^W = \frac{1}{2}\rho U_{re}^2 A_f L_v C_R(\alpha_w, \beta_w) \tag{7c}$$

$$m_{vy}^W = \frac{1}{2}\rho U_{re}^2 A_f L_v C_P(\alpha_w, \beta_w) \tag{7d}$$

$$m_{vz}^W = \frac{1}{2}\rho U_{re}^2 A_f L_v C_Y(\alpha_w, \beta_w) \tag{7e}$$

with

$$U_{re} = \sqrt{U_{xe}^2 + U_{ye}^2 + U_{ze}^2} \tag{8a}$$

$$\alpha_w = \arctan\left(\frac{\sqrt{U_{ye}^2 + U_{ze}^2}}{U_{xe}}\right) \tag{8b}$$

$$\beta_w = \arctan\left(\frac{U_{ze}}{U_{ye}}\right), \tag{8c}$$

where ρ is the density of air; A_f is a reference area; L_v is a reference length; and C_S, C_L, C_P, C_Y, and C_R are the corresponding aerodynamic coefficients, which are the functions of the equivalent yaw angle α_w and the equivalent attack angle β_w.

3.2. Random Roughness Height of Road Surface. Roughness height of a road surface is a random process in space. Generally, it is assumed as a homogeneous and ergodic random field with a Gaussian distribution [15, 16]. A one-parameter function is used to express PSD of the random road roughness in ISO 8608 [17] as

$$G(\Omega) = G(\Omega_0)\left(\frac{\Omega}{\Omega_0}\right)^{-2}, \tag{9}$$

where Ω is the spatial frequency in rad/m; Ω_0 is a fixed spatial frequency of 1 rad/m; and $G(\Omega)$ is PSD at the spatial frequency Ω. For different road conditions, different values of $G(\Omega_0)$ are defined. In ISO 8608, the road is classified into A, B, C, D, E, F, G, and H. $G(\Omega_0)$ corresponding to these grades are 1×10^{-6}, 4×10^{-6}, 16×10^{-6}, 64×10^{-6}, 256×10^{-6}, 1024×10^{-6}, 4096×10^{-6}, and 16384×10^{-6}, respectively.

An exponentially decreasing model is recommended to consider the lateral coherence of the random roughness height [18]:

$$r(\Omega) = \exp\left(-\rho_r t_w \Omega\right), \tag{10}$$

where $r(\Omega)$ is the coherence coefficient for the spatial frequency Ω; ρ_r is a parameter; and t_w is the lateral distance between paths. Following the measurement [18], ρ_r is taken as 4 in this study.

The spectral representation method proposed by Shinozuka [19] is a typical technique to generalize the random field of the roughness height. For a road surface, X represents the moving direction of the vehicle and Y represents the lateral direction. The lateral width of the road is divided into N_{ls} segments. The roughness height Z at X on the jth segment is

$$Z_j(X) = \sqrt{2(\Delta\Omega)} \sum_{m=1}^{j} \sum_{k=1}^{N} \sqrt{G(\Omega_{mk})} R(\Omega_{mk}) \cos\left(\Omega_{mk} X + \phi_{mk}\right) \tag{11a}$$

$$\Omega_{mk} = (k-1)\Delta\Omega + \frac{m}{n}\Delta\Omega \tag{11b}$$

$$R(\Omega_{mk}) = \begin{cases} 0, & \text{when } i \le j < m \le n \\ r(\Omega_{mk})^{|j-m|}, & \text{when } m = 1,\ m \le j \le n \\ r(\Omega_{mk})^{|j-m|}\sqrt{1 - r(\Omega_{mk})^2}, & \text{when } 2 \le m \le j \le n \end{cases} \tag{11c}$$

where $\Delta\Omega$ is the interval of the spatial frequency; N_{sf} is the total number of spatial frequency intervals; and ϕ_{mk} is a random phase angle uniformly distributed between 0 and 2π.

3.3. Random Parameters. Typical random variables, which may influence the wind-induced accident significantly, are the weight of the vehicle and the road friction coefficient. They are assumed as normal distribution in the previous study [8]. The driver behavior is another important factor which is related directly to the lateral motion of the vehicle. In most cases, the front wheels are steered by the driver while

the rear wheels are driven by an engine. A model is needed to provide the steering feedback from the driver. A simple and physically realistic model of driver behavior is used to control the steer angle δ of the front wheels [3], in which δ is proportional to the lateral displacement and velocity of the vehicle:

$$\delta = -\lambda_1 Y_{vb}(t-\varepsilon) - \lambda_2 v_{vbY}(t-\varepsilon), \tag{12}$$

where v_{vbY} and Y_{vb} are the velocity and the displacement from the stable lane of the vehicle body at its center in the Y-direction; λ_1 and λ_2 are two constants; and ε is the driver reaction time. To reflect the randomness of the handing by drivers, the driver reaction time is taken as random parameter in this study.

4. Dynamic Reliability Evaluation

4.1. Wind-Induced Accident Criteria and Safety Reliability. For a vehicle in winds, overturning or course deviation may happen. Course deviation means the vehicle occurring excessive lateral displacement, which may involve a collision with a vehicle in the adjacent lane or equipment on the side of the road. Overturning reflects the contacting status of the wheels with the road while course deviation represents a displacement status. A lateral displacement of 0.5 m is suggested as $Y_{\max}$, the course deviation standard, by [3] and widely accepted so far by many followers. To evaluate the overturning accident, Load Transfer Ratio (LTR [7]) defined on the vertical contact forces between the wheels and the road for the whole vehicle body can be employed as

$$\mathrm{LTR} = \frac{\sum_{j=1}^{\mathrm{nd}} f_{cdj} - \sum_{j=1}^{\mathrm{nu}} f_{cuj}}{\sum_{j=1}^{\mathrm{nd}} f_{cdj} + \sum_{j=1}^{\mathrm{nu}} f_{cuj}}, \tag{13}$$

where f_{cdj} is the contact force on the jth downwind wheel with nd being the total number of the downwind wheels; f_{cuj} is the contact force on the jth upwind wheel with nu being the total number of upwind wheels. If LTR exceeds 0.9, the vehicle is regarded as overturning in a conservative consideration.

Dynamic reliability evaluation of the road vehicle subjected to crosswinds is to assess the safety reliability probability P_r of the running vehicle under the random excitations. The safety reliability P_r for overturning and course deviation in time period T can be therefore defined as

$$P_{rO} = P\{\mathrm{LTR} < 0.9,\ 0 < t \le T\} \tag{14a}$$

$$P_{rC} = P\{|Y| < 0.5,\ 0 < t \le T\}, \tag{14b}$$

where $P\{\}$ represents the probability under the condition enclosed in {}; the subscripts O and C stand for overturning and course deviation, respectively. The typical methods to estimate the dynamic reliability are the first-passage probability, Poisson approximation, and Markov approximation. They are described as follows.

4.2. First-Passage Probability and Reliability. First-passage is a widely employed concept to obtain the dynamic reliability [20]. For a general stationary normal process g with zero mean, the probability density function at its extreme value b has the following form:

$$p(b) = \frac{\left(1-a^2\right)^{1/2}}{(2\pi)^{1/2}\sigma_g} \exp\left[-\frac{b^2}{2\sigma_g^2\left(1-a^2\right)}\right] + \frac{ab}{2\sigma_g^2} \cdot \exp\left[-\frac{b^2}{2\sigma_g^2}\right]\left[1+\mathrm{erf}\left(\frac{ab^2}{\sigma_g\left[2\left(1-\sigma_g^2\right)\right]^{1/2}}\right)\right] \tag{15}$$

with

$$a = \frac{\sigma_{\dot{g}}^2}{\sigma_g \sigma_{\ddot{g}}}, \tag{16}$$

where σ_g is the standard derivation of the process; $\sigma_{\dot{g}}$ and $\sigma_{\ddot{g}}$ are the standard derivations of the first and the second time derivatives, respectively.

For a stationary normal process with zero mean, the number of the peaks and the number of valleys are equal to each other in statistics. If n represents the number of the peaks or valleys in the process, the probability of the process below B can expressed as

$$P(g < B) = \left[\int_{-\infty}^{B} p(b)\,\mathrm{d}b\right]^n. \tag{17}$$

The probability of the process between B and $-C$ can expressed as

$$P(-C < g < B) = \left[\frac{\int_{-\infty}^{B} p(b)\,\mathrm{d}b + \int_{-\infty}^{C} p(b)\,\mathrm{d}b}{2}\right]^{2n}. \tag{18}$$

If $B = C$, there comes

$$P(-B < g < B) = \left[\int_{-\infty}^{B} p(b)\,\mathrm{d}b\right]^{2n}. \tag{19}$$

4.3. Poisson Approximation and Reliability. For a special threshold value, the first time at which the random process upcrossing is a random variable, since the upcrossing rate is independent of the past history of the process, Poisson approximation is applied to the upcrossing event in practice. The final dynamic reliability dependent for a double threshold based on Poisson assumption [20] is

$$P(-B < g < B, T) = \exp\left[-\frac{\sigma_{\dot{g}} T}{\pi\sigma_g}\exp\left(-\frac{B^2}{2\sigma_g^2}\right)\right]. \tag{20}$$

For a single threshold, the reliability is expressed as

$$P(g < B, T) = \exp\left[-\frac{\sigma_{\dot{g}} T}{2\pi\sigma_g}\exp\left(-\frac{B^2}{2\sigma_g^2}\right)\right]. \tag{21}$$

The probability of the process between B and $-C$ can expressed as

$$P(-C < g < B, T) = \exp\left\{-\frac{\sigma_{\dot{g}} T}{\pi\sigma_g}\left[\exp\left(-\frac{C^2}{2\sigma_g^2}\right) + \exp\left(-\frac{B^2}{2\sigma_g^2}\right)\right]\right\}. \tag{22}$$

4.4. Markov Approximation and Reliability. Based on a two-state Markov assumption, Vanmarcke [21] derived another typical probability of the first-passage problems. For a double threshold, the reliability is expressed as

$$P\left(-B < g < B, T\right) = \left[1 - \exp\left(-\frac{B^2}{2\sigma_g^2}\right)\right] \cdot \exp\left[-\frac{\sigma_{\dot{g}} T}{\pi \sigma_g} \cdot \exp\left(-\frac{B^2}{2\sigma_g^2}\right) \frac{1 - \exp\left(-\sqrt{\pi/2}\, q\left(B/\sigma_g\right)\right)}{1 - \exp\left(-B^2/2\sigma_g^2\right)}\right] \tag{23}$$

with the parameter

$$q = \sqrt{1 - \frac{\rho_1^2}{\rho_0 \rho_1}}, \qquad \rho_i = \int_0^\infty \omega^i G_s(\omega)\, d\omega, \tag{24}$$

where $G_s(\omega)$ is the one-sided spectral density function of the random process.

4.5. Monte Carlo Simulation and Latin Hypercube Sampling. Monte Carlo Simulation is a basic technique to judge the statistic characteristics of the stochastic responses according to the stochastic inputs. To consider the randomness during the wind-induced vehicle accident, Monte Carlo Simulation will be employed. For the random variables in this system, Latin Hypercube Sampling [22] is adopted to generate the random values to avoid too much computational effects. In this sampling, the value range of each random variable is divided into N_{sub} subranges with equal probability of $1/N_{\text{sub}}$. In each subrange, a representative value of the variable is extracted in a random way. Totally, N_{sub} representative values for all the subranges are composed to a series of the random variable. Thus, all possible values of the random variable are represented. For each representative value, a group of dynamic responses of the system can be simulated and the corresponding dynamic probability can be calculated. Based on the resultant N_{sub} groups of responses, the probability of dynamic probability can be estimated as

$$P\left(P_r \le P_{r0}\right) = \frac{\text{number of times } P_r \le P_{r0}}{N_{\text{sub}}}. \tag{25}$$

5. Numerical Implementation and Reliability Model

For a basic numerical case, a vehicle moves with a speed of 100 km/h under random crosswinds with a mean value of 10 m/s. The road surface is smooth ideally without any roughness. The reaction time of the driver is taken as 0.25 s. The velocity gain λ_2 and displacement gain λ_1 in the driver model are 0.2 and 0.7, respectively. The road friction coefficient is taken as 0.6. The vehicle weight is 4480 kg. Based on this case, the three typical dynamic reliability evaluation methods are compared. A distribution model of the dynamic reliability is then proposed for the safety evaluation of the road vehicle in turbulent winds.

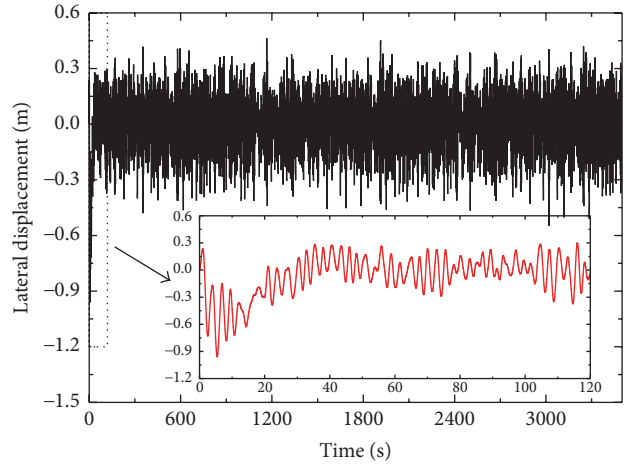

Figure 3: Time history of lateral displacement.

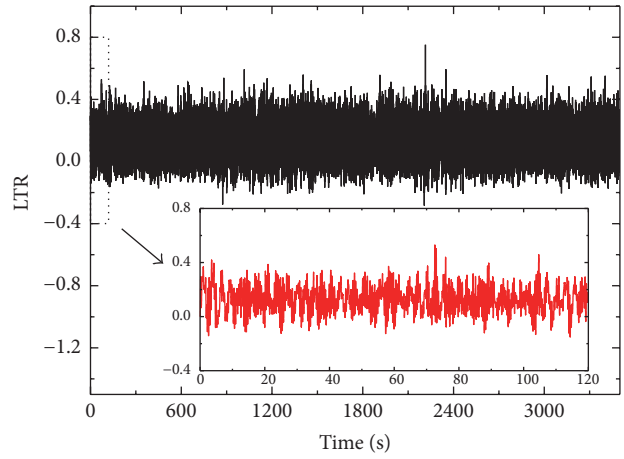

Figure 4: Time history of LTR.

5.1. Comparison of Dynamic Reliability Methods. The time history of the lateral displacement of the road vehicle is shown in Figure 3. In the first 60 s, the vehicle experiences large lateral displacement due to the crosswind loads and turns back to a normal status under the control of the driver. Later on, the vehicle moves in a relative stable trace in the lateral direction under both the crosswind and the driver. The overturning index LTR is shown in Figure 4. LTR remains fluctuating around a mean value of 0.13, which is a direct effect of the mean wind. To only consider the action of the random crosswinds, the results of the first 200 s are not included in the reliability analysis.

Using double threshold reliability expressions of the first-passage, Poisson assumption, and Markov assumption, the reliabilities of the lateral displacement on 1 km road are

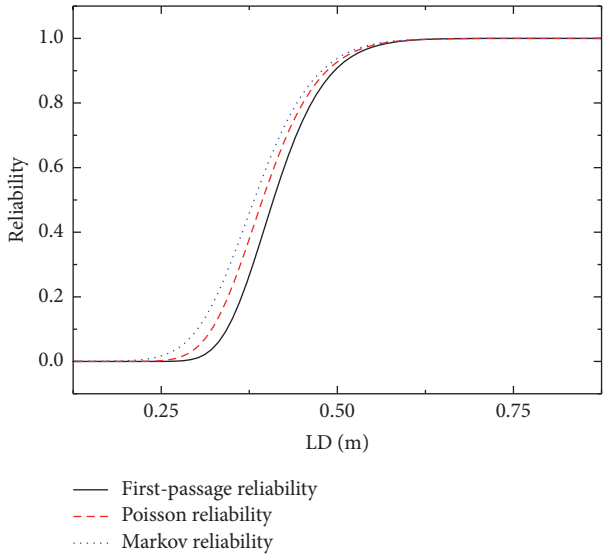

Figure 5: Reliability of lateral displacement.

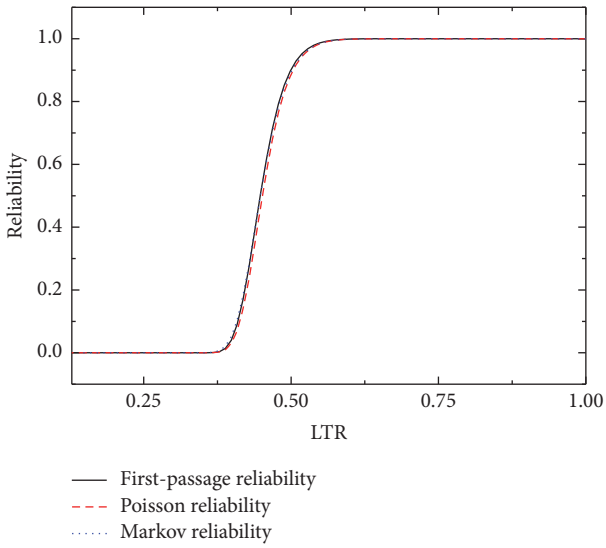

Figure 6: Reliability of LTR.

shown in Figure 5. The reliabilities from the three methods agree well with each other. For the critical value $y_{\max} = 0.5$, the corresponding reliability values are 0.908, 0.932, and 0.935, respectively. The first-passage method gives a more conservative result. The double threshold reliabilities of LTR of the vehicle for different methods on 1 km road are shown in Figure 6. Similarly, the reliabilities tend to be consistent for the three methods. However, Poisson assumption method gives a more conservative result. For a double side reliability of LTR = 0.9, the corresponding reliability values are 1.0, 1.0, and 1.0, respectively, which means the vehicle hardly overturns under this condition, which can also be reflected in the time history in Figure 4. In the following studies, the first-passage and Poisson method will be employed in consideration of the course deviation and overturning,

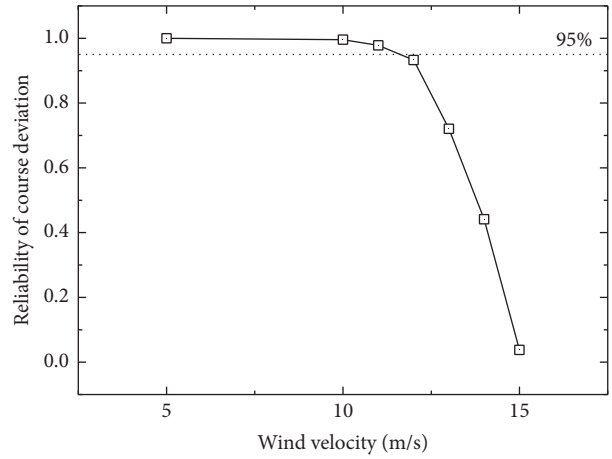

Figure 7: Reliability with wind velocity (course deviation).

respectively. In the lateral direction, the vehicle moves around the target lane (lateral displacement = 0, see Figure 3). The course deviation reliability is a double threshold issue as (14a) and (19) of the first-passage are employed. LTR fluctuates around a mean value due to the mean wind (see Figure 4). Thus, the reliability of LTR is not a double threshold issue (see (14a)) and (22) of Poisson method is employed with $C = 1$.

5.2. Effects of Single Variable. To consider the effects of mean wind velocity, the dynamic reliability of the vehicle with different mean wind velocities is calculated. The safety reliability distribution of the course deviation with the mean wind velocity is shown in Figure 7. With the increase of the mean wind velocity, the reliability decreases due to the raise of the wind loads. And the decrease rate of the reliability with the mean wind velocity increases rapidly above 10 m/s. With the mean wind velocity larger than 11.6 m/s, the course deviation reliability is lower than 95%. Around 15 m/s mean wind velocity, the reliability approaches zero. In the range of 0 and 15 m/s, the overturning reliabilities are distributed around 1 and not shown, which means the course deviation has a lower reliability and occurs before the overturning in this basic numerical case.

Beside the mean wind velocity, the reliabilities of the vehicle under the wind-induced accident criteria with the variation of the vehicle speeds are also calculated and compared. The safety reliability distribution of the course deviation with the vehicle speed is shown in Figure 8. With the increase of the vehicle speed, the wind loads on the vehicle also increase. As a direct result, the corresponding reliability decreases. The decrease rate of the reliability also grows and becomes very sharp above 90 km/h. With the vehicle speed greater than 96 km/h, the course deviation reliability is below 95%. Among 0 and 105 km/h, the reliabilities for the overturning approach 1. Similar to the situation about the mean wind velocity, course deviation is easier to appear that overturing for the vehicle in the basic case.

As described in Section 3.2, several levels of road surface are classified due to the magnitude of the PSD. At different

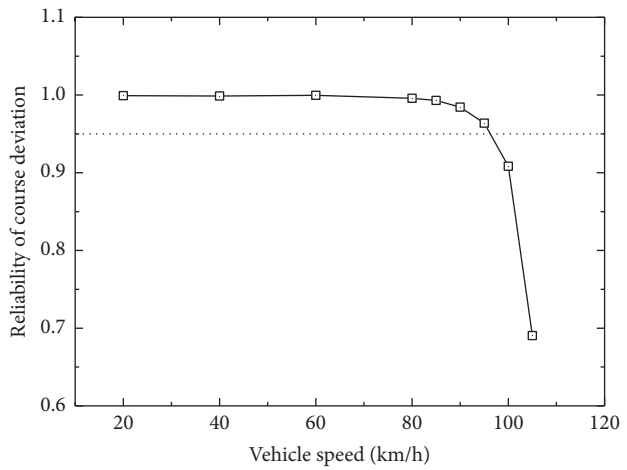

FIGURE 8: Reliability with vehicle speed (course deviation).

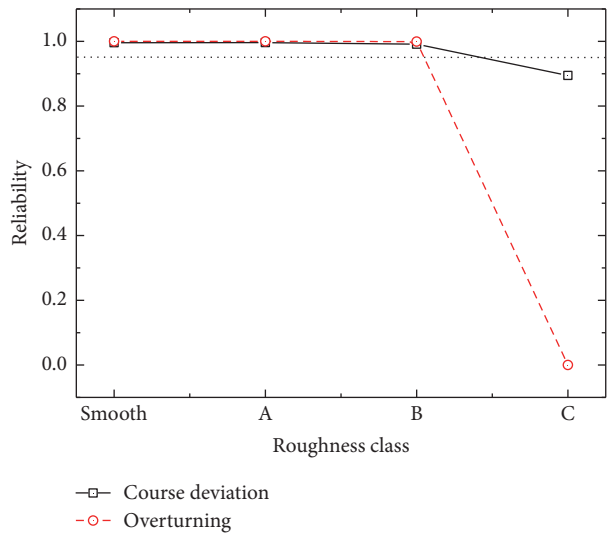

FIGURE 9: Reliability with roughness level.

roughness levels, the reliabilities of the vehicle with a moving speed of 80 km/h and mean wind velocity of 10 m/s are calculated and shown in Figure 9. In this figure, "smooth" represents the ideal road without surface roughness. From A to C, the road surface condition becomes worse. With the worsening of the road surface, the safety reliability reduces. Even at level C, the overturning reliability approaches zero. The reason is that the higher roughness heights excite more excessive vibration combined with the turbulent winds, which leads to be more unsafe. In this regard, worse road surface conditions from D to E in ISO 8608 are not studied.

The friction coefficient, driver reaction time, and vehicle weight are accepted as random variables with normal distribution in this study. Their standard deviations are assumed as 10% of their mean values. For each of them, 50 samples are obtained through Latin Hypercube Sampling. At each sample, the wind-induced reliability can be calculated based on the dynamic responses of the lateral displacement and LTR. For the vehicle moving on a smooth road with a speed of 80 km/h and mean wind velocity of 10 m/s, the probability distribution of the safety reliability corresponding to each random variable can be gained through (25). Figure 10 shows the probability distribution of the course deviation reliability with the friction coefficient, driver reaction time, and vehicle weight. Driver reaction has the highest width of reliability while the friction coefficient has the lowest one. Therefore, in the three random variables, the driver behavior takes a higher role in the course deviation of the vehicle accident during crosswinds. For the overturning accident, the reliability for each sample approaches 1 and is not shown.

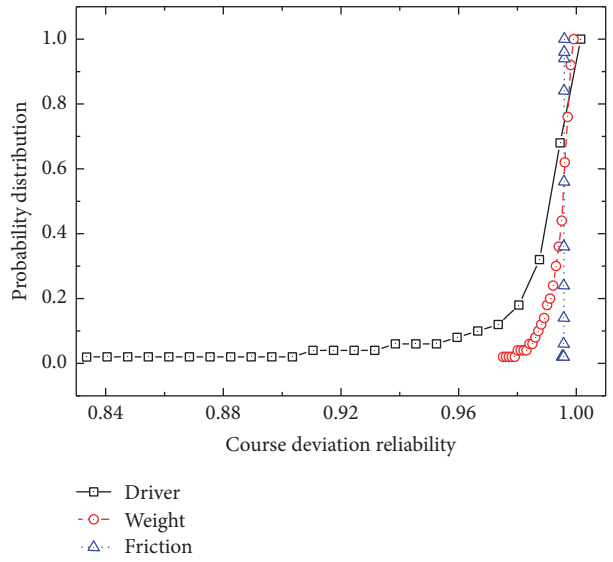

FIGURE 10: Probability distribution of reliability (course deviation).

5.3. Reliability Model. To describe the probability distribution of the reliability with the random variables, a modified Lorentz profile is proposed. A basic Lorentz profile is expressed as [23]

$$y_L = \frac{I_0}{1 + \left[2\left(x_L - x_{L0}\right)/\Delta_L\right]^2}, \tag{26}$$

where I_0 is the intensity (maximum value) at the center position ($x_L = x_{L0}$) and Δ_L is the full-width at half-maximum ($I_0/2$). Adding an offset y_{L0} to consider the possible offset due to the possible numerical errors, (26) becomes

$$y_L = y_{L0} + \frac{I_0}{1 + \left[2\left(x_L - x_{L0}\right)/\Delta_L\right]^2}. \tag{27}$$

In consideration of the probability distribution, the maximum value I_0 is 1 and the corresponding center x_{L0} is also 1. Therefore, (27) becomes

$$y_L = y_{L0} + \frac{1}{1 + \left[2\left(x_L - 1\right)/\Delta_L\right]^2}. \tag{28}$$

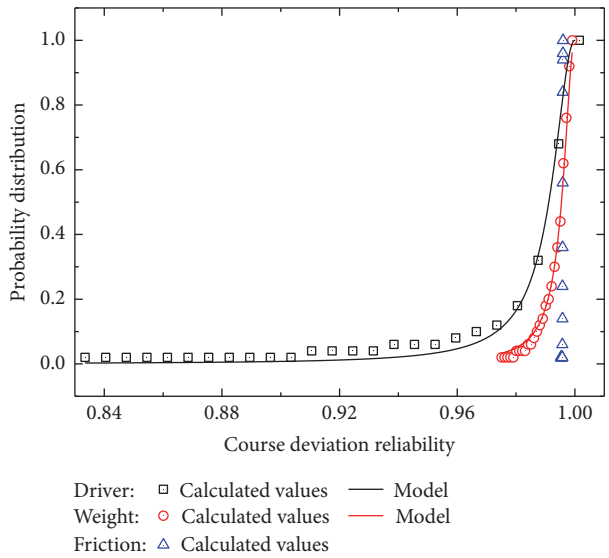

Figure 11: Probability distribution model of reliability.

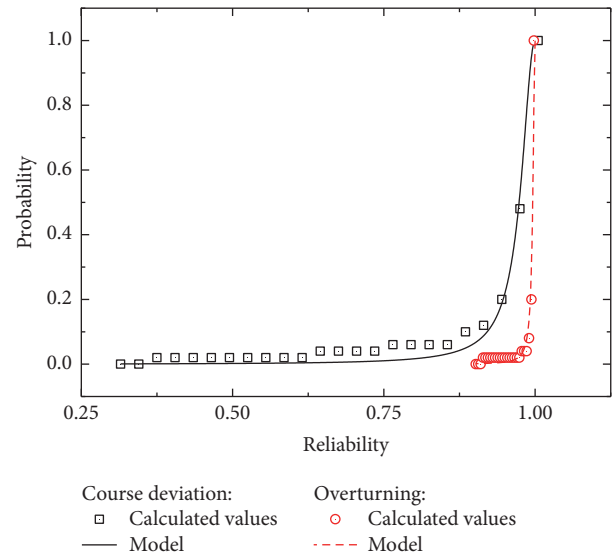

Figure 12: Probability distribution of reliability (combined random conditions).

For $x_L = 0$, the probability is also 0. Thus,

$$y_{L0} = -\frac{1}{1 + \left[2/\Delta_L\right]^2}. \tag{29}$$

The final form of the modified Lorentz profile for the reliability distribution is

$$y_{\mathrm{LM}} = \frac{1}{1 + \left[2\left(x_L - 1\right)/\Delta_L\right]^2} - \frac{1}{1 + \left[2/\Delta_L\right]^2} \tag{30}$$

with a single parameter Δ_L.

To check the appropriateness of this model, the probability results in Figure 10 are fitted using (30) and shown in Figure 11. For the friction coefficient, the probability distributions are located in the very narrow reliability range and are not fitted. For the random driver and weight, the model parameters are 0.0178 and 0.0091, respectively. From Figure 11, the modified Lorentz profile can be employed appropriately.

5.4. Safety Index and Evaluation. Δ_L in the probability distribution model (see (30)) can not only reflect the width of the reliability distribution, but also be taken as a safety index. For a given reliability distribution value y_g, the reliability can be solved as

$$x_g = 1 - \frac{\Delta_L}{2}\sqrt{\frac{1}{y_g + 1/\left(1 + \left[2/\Delta_L\right]^2\right)} - 1}. \tag{31}$$

Generally taking $y_g = 95\%$ and $x_g \leq 0.95$ as the accepted safety reliability for the wind-induced vehicle accident, the safety index can be derived from (31) as $\Delta_L \leq 0.023$. Just comparing the magnitude of the model parameter with 0.023, the accepted wind-induced vehicle safety can be determined directly. As the vehicle moves on a B level road surface with a speed of 80 km/h and mean wind velocity of 10 m/s, the reliability distribution on the combined randomness of the friction coefficient, the driver reaction time, and the vehicle weight are shown in Figure 12. Δ_L for the course deviation and the overturning are 0.053 and 0.008, respectively. Compared with the safety value 0.023, the reliability of the course deviation is very big and not accepted while the overturning can be accepted.

6. Conclusion

In this study, the dynamic responses of a road vehicle moving under turbulent winds are solved based on a nonlinear vibration system of the vehicle. The dynamic reliabilities of the wind-induced safety in crosswinds are explored using three typical methods, the first-passage, Poisson assumption, and Markov assumption. Through comparisons, the first-passage method provides a conservative result for the course deviation reliability while Poisson assumption method gives a conservative reliability for the overturning. For a basic numerical case, the reliability decreases with the increase of the mean wind velocity, the vehicle speed, and the road roughness height. Particularly, there exist some critical statuses where the dynamic reliability changes in a sharp rate. For an ideally smooth road, the safety reliability of the course deviation is lower than the one of the overturning, which is opposite for high roughness road. Monte Carlo Simulation with Latin Hypercube Sampling is employed to find out the random variables such as the vehicle weight, road friction coefficient, and the driver reaction time on the dynamic reliability. Of them, the driver behavior takes higher role in the course deviation. Eventually, a distribution model with modified Lorentz profile for the dynamic reliability is proposed. In this model, only a single parameter is needed and it can be used as a safety index to evaluate the dynamic reliability. With a given reliability bound, whether the safety

status can be accepted can be easily decided from this safety index. It is unfortunate that the corresponding experimental data are few to give an adequate verification, which is a general limitation for the simulation of such complex wind-vehicle effects. The full process and method about the dynamic reliability evaluation, probability distribution, and its model would be referred basically for the further study or application in the concept of dynamic reliability.

Nomenclature

A_f: The reference area
b: The extreme value
b_1: The half distance between the wheels on the same axle
B: A supposed value
C: A supposed value
C_L: The aerodynamic coefficient for lift force
C_S: The aerodynamic coefficient for side force
erf(): Gauss error function
f: The nondimensional normalized frequency
f_{cdj}: The contact force on the jth downwind wheel from the road
f_{cuj}: The contact force on the jth upwind wheel from the road
f_{vby}^G: The gravity component on the vehicle body along y-axis
f_{vbz}^G: The gravity component on the vehicle body along z-axis
f_{wiy}^S: The force component passed between the vehicle body and the ith wheel along y-axis
f_{wiz}^S: The force component passed between the vehicle body and the ith wheel along z-axis
f_{vy}^W: The component of wind-induced force on the vehicle body along y-axis
f_{vz}^W: The component of wind-induced force on the vehicle body along z-axis
G: PSD of the random road roughness
G_s: The one-sided spectral density function of a random process
h_1: The distance between the plane of the wheel center and the gravity center of the vehicle body
I_0: The intensity at $x_L = x_{L0}$ in Lorentz profile
I_{xx}: The mass moment component of inertia of the vehicle body along x-axis
I_{xz}: The product of inertia in xz plane
I_{yy}: The mass moment component of inertia of the vehicle body along y-axis
I_{zz}: The mass moment component of inertia of the vehicle body along z-axis
K: The Von Kármán number
L_1: The distance between the front wheel axle and the gravity center of the vehicle body
L_2: The distance between the rear wheel axle and the gravity center of the vehicle body
L_v: The reference length
LTR: Load Transfer Ratio
m_{vb}: The mass of the vehicle body
m_{vx}^W: The wind-induced moment component on the vehicle body along x-axis
m_{vy}^W: The wind-induced moment component on the vehicle body along y-axis
m_{vz}^W: The wind-induced moment component on the vehicle body along z-axis
M_P: Aerodynamic coefficient for pitching moment
M_R: Aerodynamic coefficient for rotating moment
M_Y: Aerodynamic coefficient for yawing moment
n: The number of the peaks or valleys in a process
n_f: The frequency in Hz
N: The total number of frequency intervals
N_{ls}: The number of the segments in the lateral for road surface simulation
N_{sf}: The total number of spatial frequency intervals for road surface simulation
N_{sub}: The number of the subranges for a random variable
nd: The total number of the downwind wheels
nu: The total number of upwind wheels
$p()$: The probability density function
$P()$: The probability function
P_r: The safety reliability probability
P_{rC}: The safety reliability P_r for course deviation
P_{rO}: The safety reliability P_r for overturning
q: The parameter in the reliability based on Markov approximation
r: The coherence coefficient for the road roughness
S_u: The power spectrums of u
S_v: The power spectrums of v
t_w: The lateral distance between paths
T: The time period
u: The turbulent wind velocity component in the direction of the mean wind
u_*: The shear velocity of the flow
U: The mean velocity
U_{re}: The equivalent natural wind component
U_{xe}: The natural wind component along x-axis
U_{ye}: The natural wind component along y-axis
U_{ze}: The natural wind component along z-axis
v: The turbulent wind velocity component in the direction vertical to the mean wind
v_{vbx}: The translational velocity component of the vehicle body along x-axis
v_{vby}: The translational velocity component of the vehicle body along y-axis
v_{vbY}: The translational velocity component the vehicle body in the Y-direction

v_{vbz}: The translational velocity component of the vehicle body along z-axis
$\dot{v}_{vby}$: The translational acceleration component of the vehicle body along y-axis
$\dot{v}_{vbz}$: The translational acceleration component of the vehicle body along z-axis
V: The vehicle speed
V_r: The equivalent wind velocity for the mean wind
x: A direction in the Cartesian coordinate system founded on the gravity center of the vehicle body
x_g: The reliability related to the given reliability distribution value y_g
x_L: The variable in Lorentz profile related to the position
x_{L0}: The center value of x_L
X: The moving direction of the vehicle
y: Three directions in the Cartesian coordinate system founded on the gravity center of the vehicle body
y_g: A given reliability distribution value
y_L: Lorentz profile
y_{LM}: The modified Lorentz profile
Y: The lateral direction of the vehicle and vertical to X in the horizontal plane
Y_{vb}: The displacement from the stable lane of the vehicle body in Y-direction
z: A direction in the Cartesian coordinate system founded on the gravity center of the vehicle body
z_h: The height from the ground
z_0: The roughness height of the ground
Z: The roughness height of the road surface
α_w: The equivalent yaw angle of the natural wind to the vehicle
β_w: The equivalent attack angle of the natural wind to the vehicle
δ: The steer angle of the front wheels
Δ_L: The full-width at half-maximum in Lorentz profile
Δn: The frequency interval
$\Delta\Omega$: The interval of Ω
ε: The driver reaction time
λ_1: Constant 1 in the drive model
λ_2: Constant 2 in the drive model
π: The circumference ratio
ρ: The density of air
ρ_i: The integration of the function of ω and G
ρ_r: The parameter in the exponentially decreasing model for road roughness
σ_g: The standard derivations of the process g
$\sigma_{\dot{g}}$: The standard derivation of the first time derivative of the process g
$\sigma_{\ddot{g}}$: The second derivation of the first time derivative of the process g
φ: The angle between the mean velocity vector and the vehicle speed vector
ϕ_u: The random phase angle for the simulation of u
ϕ_v: The random phase angle for the simulation of v
ϕ_{mk}: The random phase angle for road surface simulation
ω: The circular frequency
ω_{vbx}: The angular velocity component of the vehicle body along x-axis
ω_{vby}: The angular velocity component of the vehicle body along y-axis
ω_{vbz}: The angular velocity component of the vehicle body along z-axis
$\dot{\omega}_{vbx}$: The angular acceleration component of the vehicle body along x-axis
$\dot{\omega}_{vby}$: The angular acceleration component of the vehicle body along y-axis
$\dot{\omega}_{vbz}$: The angular acceleration component of the vehicle body along z-axis
Ω: The spatial frequency in rad/m
Ω_0: The fixed spatial frequency of 1 rad/m
∞: Infinity.

Competing Interests

The authors declare that there is no conflict of interests regarding the publication of this paper.

Acknowledgments

The authors are grateful for the financial supports from the open project of the Transport Industry Key Laboratory for Wind Resistance Technique in Bridge Engineering (KLWRTBMC14-02), the Fundamental Research Funds for the Central Universities (2682016CX018), and the National Natural Science Foundation of China (51508480) to the first author and the Applied Basic Research Projects of the Ministry of Transport (2014319J13100), the Sichuan Province Youth Science and Technology Innovation Team (2015TD0004), and the National Science Fund for Distinguished Young Scholars (51525804) to the second author.

References

[1] C. J. Baker and S. Reynolds, "Wind-induced accidents of road vehicles," *Accident Analysis & Prevention*, vol. 24, no. 6, pp. 559–575, 1992.
[2] C. S. Cai, J. Hu, S. Chen, Y. Han, W. Zhang, and X. Kong, "A coupled wind-vehicle-bridge system and its applications: a review," *Wind and Structures*, vol. 20, no. 2, pp. 117–142, 2015.
[3] C. J. Baker, "High sided articulated road vehicles in strong cross winds," *Journal of Wind Engineering and Industrial Aerodynamics*, vol. 31, no. 1, pp. 67–85, 1988.
[4] F. Cheli, P. Belforte, S. Melzi, E. Sabbioni, and G. Tomasini, "Numerical-experimental approach for evaluating cross-wind aerodynamic effects on heavy vehicles," *Vehicle System Dynamics*, vol. 44, Supplement 1, pp. 791–804, 2006.
[5] S. Chen and F. Chen, "Simulation-based assessment of vehicle safety behavior under hazardous driving conditions," *Journal of Transportation Engineering*, vol. 136, no. 4, pp. 304–315, 2010.

[6] Y. L. Xu and W. H. Guo, "Dynamic behaviour of high-sided road vehicles subject to a sudden crosswind gust," *Wind and Structures*, vol. 6, no. 5, pp. 325–346, 2003.

[7] B. Wang, Y. Xu, and Y. Li, "Nonlinear safety analysis of a running road vehicle under a sudden crosswind," *Journal of Transportation Engineering*, vol. 142, no. 2, Article ID 04015043, 2016.

[8] R. Sigbjörnsson and J. T. Snæbjörnsson, "Probabilitic assessment of wind related accidents of road vehicles: a reliability approach," *Journal of Wind Engineering and Industrial Aerodynamics*, vol. 74–76, pp. 1079–1090, 1998.

[9] F. Chen and S. Chen, "Reliability-based assessment of vehicle safety in adverse driving conditions," *Transportation Research Part C: Emerging Technologies*, vol. 19, no. 1, pp. 156–168, 2011.

[10] C. Proppe and C. Wetzel, "A probabilistic approach for assessing the crosswind stability of ground vehicles," *Vehicle System Dynamics*, vol. 48, supplement 1, pp. 411–428, 2010.

[11] S. Emil and R. H. Scanlan, *Wind Effects on Structures: Fundamentals and Applications to Design*, John Wiley & Sons, Hoboken, NJ, USA, 3rd edition, 1996.

[12] J. C. Kaimal, J. C. Wyngaard, Y. Izumi, and O. R. Coté, "Spectral characteristics of surface-layer turbulence," *Quarterly Journal of the Royal Meteorological Society*, vol. 98, no. 417, pp. 563–589, 1972.

[13] G. I. Taylor, "The spectrum of turbulence," *Proceedings of the Royal Society A: Mathematical, Physical and Engineering Sciences*, vol. 164, no. 919, pp. 476–490, 1938.

[14] M. Wu, Y. Li, X. Chen, and P. Hu, "Wind spectrum and correlation characteristics relative to vehicles moving through cross wind field," *Journal of Wind Engineering and Industrial Aerodynamics*, vol. 133, pp. 92–100, 2014.

[15] L. Sun and X. Deng, "Predicting vertical dynamic loads caused by vehicle-pavement interaction," *Journal of Transportation Engineering*, vol. 124, no. 5, pp. 470–477, 1998.

[16] K. M. A. Kamash and J. D. Robson, "The application of isotropy in road surface modelling," *Journal of Sound and Vibration*, vol. 57, no. 1, pp. 89–100, 1978.

[17] ISO, "Mechanical vibration-road surface profiles-reporting of measured data," ISO 8608, 1995.

[18] K. Bogsjö, "Coherence of road roughness in left and right wheelpath," *Vehicle System Dynamics*, vol. 46, supplement 1, pp. 599–609, 2008.

[19] M. Shinozuka, "Simulation of multivariate and multidimensional random processes," *Journal of the Acoustical Society of America*, vol. 49, no. 1, pp. 357–368, 1971.

[20] L. D. Lutes and S. Sarkani, *Random Vibrations, Analysis of Structural and Mechanical Systems*, Elsevier Butterworth-Heinemann, Burlington, Mass, USA, 2004.

[21] E. H. Vanmarcke, "On the distribution of the first-passage time for normal stationary random processes," *Journal of Applied Mechanics*, vol. 42, no. 1, pp. 215–220, 1975.

[22] M. D. McKay, R. J. Beckman, and W. J. Conover, "A comparison of three methods for selecting values of input variables in the analysis of output from a computer code," *Technometrics*, vol. 21, no. 2, pp. 239–245, 1979.

[23] A. G. Michette and S. J. Pfauntsch, "Laser plasma X-ray line spectra fitted using the Pearson VII function," *Journal of Physics D: Applied Physics*, vol. 33, no. 10, pp. 1186–1190, 2000.